

Kinetics of the two-dimensional long-range Ising model at low temperatures

Ramgopal Agrawal,^{1,*} Federico Corberi^{2,†} Eugenio Lippiello^{3,‡} Paolo Politi^{4,5,§} and Sanjay Puri^{1,||}

¹*School of Physical Sciences, Jawaharlal Nehru University, New Delhi 110067, India*

²*Dipartimento di Fisica “E. R. Caianiello”; INFN, Gruppo Collegato di Salerno; and CNISM, Unità di Salerno, Università di Salerno, Via Giovanni Paolo II 132, 84084 Fisciano, Salerno, Italy*

³*Dipartimento di Matematica e Fisica, Università della Campania, Viale Lincoln 5, 81100 Caserta, Caserta, Italy*

⁴*Istituto dei Sistemi Complessi, Consiglio Nazionale delle Ricerche, Via Madonna del Piano 10, 50019 Sesto Fiorentino, Tuscany, Italy*

⁵*INFN, Sezione di Firenze, Via G. Sansone 1, 50019 Sesto Fiorentino, Tuscany, Italy*



(Received 9 November 2020; revised 14 December 2020; accepted 23 December 2020; published 11 January 2021)

We study the low-temperature domain growth kinetics of the two-dimensional Ising model with long-range coupling $J(r) \sim r^{-(d+\sigma)}$, where $d = 2$ is the dimensionality. According to the Bray-Rutenberg predictions, the exponent σ controls the algebraic growth in time of the characteristic domain size $L(t)$, $L(t) \sim t^{1/z}$, with growth exponent $z = 1 + \sigma$ for $\sigma < 1$ and $z = 2$ for $\sigma > 1$. These results hold for quenches to a nonzero temperature $T > 0$ below the critical temperature T_c . We show that, in the case of quenches to $T = 0$, due to the long-range interactions, the interfaces experience a drift which makes the dynamics of the system peculiar. More precisely, we find that in this case the growth exponent takes the value $z = 4/3$, independently of σ , showing that it is a universal quantity. We support our claim by means of extended Monte Carlo simulations and analytical arguments for single domains.

DOI: [10.1103/PhysRevE.103.012108](https://doi.org/10.1103/PhysRevE.103.012108)

I. INTRODUCTION

After a quench from the disordered phase above the critical temperature T_c to a final temperature $T < T_c$, ferromagnetic materials undergo phase ordering [1–5]. The system orders locally inside domains whose typical size $L(t)$ grows in time until equilibration takes place on a timescale τ_{eq} which diverges with the system (linear) size \mathcal{L} . This relaxation process is called coarsening and it is often accompanied by a dynamical scaling symmetry, which amounts to the physical fact that configurations at different times are statistically similar upon measuring distances in units of $L(t)$. The latter usually increases algebraically, $L(t) \sim t^{1/z}$, where z is a nonequilibrium dynamical exponent that is unrelated to any equilibrium property. This exponent is also independent of the quench temperature [2,6], a property which is true for any universal quantity, because it can be shown that temperature is an irrelevant parameter in the sense of the renormalization group [6]. This statement applies for quenches to $0 < T < T_c$: Indeed, when cooling down to $T = T_c$ the process is qualitatively different because the order parameter vanishes in the target equilibrium state, at variance with what happens when $T < T_c$. Quenches to $T = 0$, on the other hand, may also have peculiar properties because any activated process is forbidden. To

be concrete, let us discuss a system with a scalar nonconserved order parameter.

Short-range systems. If interactions are restricted to nearest-neighbor (NN) spins, the Ising model with Glauber single-spin-flip kinetics [7] represents an appropriate description. Letting space dimension $d > 1$ above the lower critical one, in order to have a finite T_c , after quenching to $0 < T < T_c$, ordered domains grow at late times with $z = z_{\text{CD}} = 2$ until the system eventually attains the equilibrium state in a time τ_{eq} which is in most cases $\tau_{\text{eq}} \sim \mathcal{L}^z$. We indicate with z_{CD} this value of z because the motion of the interface in this case is curvature driven [2,8].

For quenches to $T = 0$, even if the motion of interfaces is no longer curvature driven but has a diffusive character, one still observes a growth law with an exponent $z = z_{\text{diff}} = z_{\text{CD}} = 2$. Another difference between $T = 0$ and $T > 0$ is that the equilibration in the former quench may be impeded due to blocking of the system into infinitely lived metastable states [9,10]. In $d = 2$ these blocked states are stripes with flat interfaces extending along the lattice directions, such as that in Fig. 1(a). Clearly, the fact that such flat interfaces are frozen affects not only the fate of the system in a quench to $T = 0$, but also the preceding dynamics. Indeed, it was shown in [11] that, although the value of z does not change in going from $T > 0$ to $T = 0$, since $z_{\text{diff}} = z_{\text{CD}}$, some other nonequilibrium exponents related to the geometry of interfaces do change.

Furthermore, even if the quench is made to a finite T , the different dynamics associated with $T = 0$ is observed in a preasymptotic regime which can be rather long if T is small enough. Similarly, for sufficiently low $T > 0$, although the metastable states are eventually escaped, this happens on timescales that can be huge, greatly delaying the equilibration

*ramgopal.sps@gmail.com

†corberi@sa.infn.it

‡eugenio.lippiello@unicampania.it

§paolo.politi@cnr.it

||purijnu@gmail.com

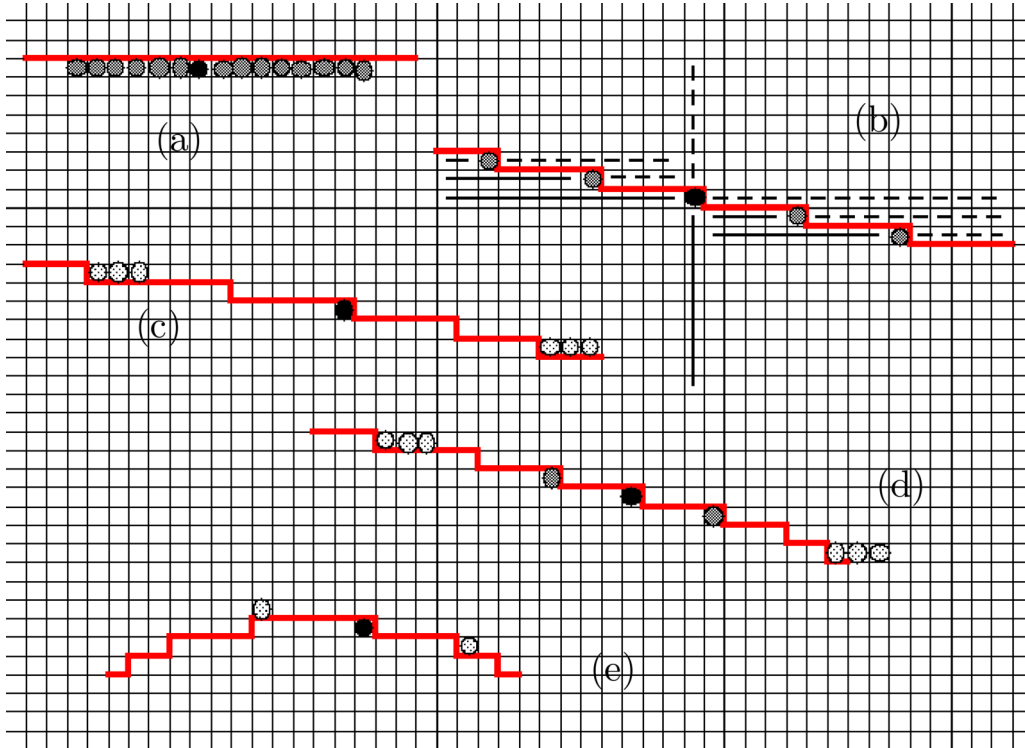


FIG. 1. Pictorial representation of different interfaces (thick red lines) on a square lattice and their stability with long-range interactions. Spins are located in the center of the small squares forming the lattice and they have opposite orientation on the two sides of the interface, supposed to extend indefinitely. We show (a) a flat interface directed along one lattice direction; (b) an interface with a constant slope (i.e., all steps have the same length); (c) an interface of positive curvature (i.e., steps become shorter upon going right); (d) an interface with a local constant slope, then acquiring a finite curvature (the three central terraces have the same length, higher terraces have an increasing length, and lower terraces have a decreasing length); and (e) an interface whose slope changes sign. For any shape we focus on a given spin on the interface (closed black circle \bullet) and we wonder about its stability at $T = 0$. Using symmetry considerations, it is possible to compensate the interaction with spins of opposite orientations. This is explicitly depicted in (b), where the interaction with spins parallel to \bullet (straight segments) is compensated with the interaction with spins antiparallel to \bullet (dashed segments). In particular, all spins within the two perpendicular straight segments originating in \bullet are compensated by all spins within the two perpendicular dashed segments originating at the same site. Once this procedure is completed, uncompensated spins are shown as dark gray circles if they are parallel to \bullet (therefore, they are stabilizing) and as light gray circles if they are antiparallel to \bullet (therefore, they are destabilizing). Therefore, spins \bullet at interfaces (a) and (b) are stable while spin \bullet in (c) is unstable. Notice that all the above is true for any value of σ . The stability of spin \bullet in (d) is more complicated because it has short-distance stabilizing interactions (dark gray circles) and longer-distance destabilizing interactions (light gray circles). The resulting effect depends on the details of the interface and on σ : For large σ we expect the short-distance stabilizing interactions to prevail, while for small σ we expect the longer-distance destabilizing interactions to do so. Finally, in (e) the edge spins of a top terrace are unstable, showing that curvature is more relevant than the sign of the slope. In all figures (b)–(e) the spin at the right of \bullet (i.e., the spin on the other side of the interface) is stable. For the NN model the picture is different because the interaction is local and the curvature is irrelevant: Interface (a) is stable while edge spins in (b)–(e) are (energetically) in neutral equilibrium, and therefore are dynamically unstable [see Eq. (3) with $\Delta E = 0$].

with respect to what happens at higher T where, as already mentioned, $\tau_{\text{eq}} \sim \mathcal{L}^z$. Summarizing, the case with $T = 0$ displays peculiar features which can strongly affect even the dynamics of quenches to finite T , at least preasymptotically.

A separated discussion is deserved by the case $d = 1$, because here $T_c = 0$, meaning that, strictly speaking, $T = 0$ is the only possibility to cool the system to a magnetized state. However, even for quenches to a finite T , a coarsening stage takes place because domains keep growing as in a $T = 0$ quench until their size $L(t)$ reaches the equilibrium correlation length ξ or the system size \mathcal{L} , after which equilibration occurs. Also in this case the motion of interfaces has a diffusive character and one finds $z = z_{\text{diff}} = 2$ [7], but, at variance with higher dimensions, there are no metastable states due to the trivial one-dimensional lattice geometry.

Long-range systems. The presence of long-range interactions changes considerably the above picture. The equilibrium scenario with a coupling between spins at distance r decaying as $r^{-(d+\sigma)}$ is well understood. There is an ordered phase below a finite T_c also in $d = 1$ provided, in this case, that $\sigma \leq 1$. Furthermore, the energy is extensive and the system is additive for any d if $\sigma > 0$, a regime sometimes referred to as a weak long-range regime, whereas extensivity and additivity are lost for $\sigma \leq 0$, the strong long-range case. In this paper we will only focus on the weak long-range case $\sigma > 0$.

Regarding the nonequilibrium properties, in quenches to a finite T one finds [12–14] $z = z_{\text{adv}} = 1 + \sigma$ for $\sigma \leq 1$ and $z = 2$ for $\sigma > 1$ (with logarithmic corrections right at $\sigma = 1$). This applies down to $d = 1$ where, if $\sigma > 1$, one has $T_c = 0$ and the discussion made above for short-range interactions

regarding equilibration applies. The different behavior of the exponent z in crossing $\sigma = 1$ can be ascribed to qualitatively different underlying dynamical mechanisms. When, for $\sigma > 1$, z takes the same value $z = 2$ as in the case with NN interactions, the motion of interfaces behaves as for NN interactions, namely, it is diffusive for $d = 1$ and is governed by the curvature [12,15] for $d > 1$. Instead, when $z = z_{\text{adv}}$, i.e., for $\sigma \leq 1$, the motion of domains walls is advected by the drift due to the long-range interactions between far away spins. Note that one has $z \rightarrow z_{\text{ball}} = 1$ for $\sigma \rightarrow 0^+$. This case corresponds to an advection of interfaces so strong as to produce a completely deterministic motion and hence a ballistic regime. This is related to the crossover from weak long-range to strong long-range interactions occurring right at $\sigma = 0$.

Regarding the differences between $T > 0$ and $T = 0$ when long-range interactions are present, the situation is not clear at all. To date, the matter has been well understood only in $d = 1$ [16–18]. In this case, when quenching to $T = 0$, one finds coarsening with $z = z_{\text{ball}} = 1$ for any σ . Let us recall that, instead, for $T > 0$ one has $z \rightarrow 1$ only in the limit $\sigma \rightarrow 0^+$. The interpretation is as follows: When $T > 0$ thermal fluctuation randomize the displacement of interfaces and therefore the motion is not fully deterministic, although still advected. In this case, in order to have full determinism, one has to go to the strong-interaction limit $\sigma \rightarrow 0$. Instead, when $T = 0$, even a relatively small drift, present for any $\sigma \leq 1$, leads to a deterministic motion with $z = z_{\text{ball}} = 1$. Also in this case, the asymptotic ballistic growth which sets in at $T = 0$ is observed as a preasymptotic behavior after quenches to finite T for any σ . Finally, let us mention that also with long-range interactions, as in the NN case, metastability is not observed in $d = 1$.

In this paper we take a step in the direction of understanding the ordering kinetics after quenches to $T = 0$ of systems with long-range interactions in $d > 1$. The matter, which is largely unexplored, is relevant because in this case, as we will illustrate, the dynamical mechanism is different from the ones discussed above, thus producing a different value $z = \mathcal{Z}$ of the growth exponent. This is independent of σ and characterizes also the preasymptotic evolution in deep quenches to a finite T .

The origin of this growth mechanism can be traced back to metastable configurations. In order to discuss this point we invite the reader to refer to Fig. 1 as a preliminary illustration of the various shapes of the interfaces, leaving further details contained in this figure, described in the detailed caption, to the specific discussion that will be conducted in Sec. IV B. As discussed previously, in $d > 1$ with NN interactions a flat portion of an interface along a lattice direction [Fig. 1(a)] is stable at $T = 0$. However, interfaces are never perfectly flat nor are they aligned along the lattice directions in the coarsening stage, and hence they can be deformed by flipping spins on the edges [Figs. 1(b)–1(d)]. This process typically occurs without any drift and hence has a diffusive character [11], a fact that leads to an exponent $z = z_{\text{diff}} = 2$. The addition of long-range interactions changes the situation in two fundamental respects. The first modification is an increase of (meta)stable configurations: Any globally straight interface [e.g., the one of Fig. 1(b), where all steps have the same size] is now locally stable, even if its direction does not fit the

orientation of the underlying lattice. This means that also spins on edges can be blocked, at variance with the NN case. Second, if we perturb the constant slope interface [e.g., see Figs. 1(c) and 1(d), where steps have different lengths], spins which are now free to flip are subjected to a deterministic drift, similarly to what happens in $d = 1$ in the ballistic regime. These two ingredients have, so to say, contrasting effects. On the one hand, the presence of the drift tends to speed the kinetics with respect to a diffusive case, leading to $z < 2$; on the other hand, the drift is contrasted by the abundance of blocked states, causing $z > 1$. The result is a nontrivial value $z = \mathcal{Z}$, with $1 < \mathcal{Z} < 2$. Even if this regime is observed unambiguously in numerical simulation, a precise determination of \mathcal{Z} is difficult with this technique also because a preasymptotic stage is present. A direct analytical attack of the problem seems to be difficult as well. This is due to the presence of long-range correlations which mix up with lattice effects making calculations elusive. Indeed, as we will discuss further, an approach on the continuum, i.e., off-lattice, which accurately captures the asymptotic values z_{adv} and z_{diff} in quenches to finite T , provides a wrong value of \mathcal{Z} . Considering instead a simplified system with a single domain, we are able to obtain a full analytic understanding of the early stage where $\mathcal{Z} = 3/2$ and a quite clean numerical determination of its asymptotic one with $\mathcal{Z} = 4/3$. While the former value can be traced back to a relatively simple circular geometry of the growing domains, the latter originates from a more peculiar one caused by the long-range interactions extending along the interfaces.

This paper is organized as follows. In Sec. II we introduce the kinetic model we study, discuss the implementation of the numerical simulations, and define the basic observable quantities we compute. Section III presents the results of numerical simulations of the model and the determination of the exponent \mathcal{Z} . In Sec. IV we simplify the problem by considering the evolution of a single domain. This is studied both numerically and analytically, allowing us to determine \mathcal{Z} . In Sec. V we summarize the main results and discuss some open points. In the Appendix we give some details of the numerical technique, namely, Ewald summation, to incorporate long-range interactions in the system.

II. MODEL AND ITS NUMERICAL SIMULATION

We consider an Ising model with the Hamiltonian

$$\mathcal{H}(\{s_i\}) = -\frac{1}{2} \sum_i \sum_j' J(r) s_i s_j, \quad (1)$$

where $s_i = \pm 1$ are Boolean spin variables on the sites i of a two-dimensional square lattice of linear size \mathcal{L} , whose spacing we assume to be unitary. The sum over j is primed to indicate that the terms with $i = j$ are excluded and

$$J(r) = r^{-(2+\sigma)} \quad (2)$$

is a ferromagnetic coupling constant with $r = |\vec{r}_i - \vec{r}_j|$, \vec{r}_i being the coordinate of site i of the lattice. The usual NN Ising model arises on setting $J(r) = \delta_{r,1}$.

At equilibrium the long-range model has a paraferromagnetic phase transition at a finite critical temperature

$T_c(\sigma)$. Critical exponents match [19–24] those of the corresponding NN model for sufficiently large values of σ , i.e., $\sigma \geq \sigma_{\text{NN}}$, where σ_{NN} has been estimated [21,24] to be $\sigma_{\text{NN}} = 7/4$, whereas they match the mean field values for $\sigma < 1$. In between, for $1 < \sigma < \sigma_{\text{NN}}$, critical exponents depend continuously on σ .

A kinetics is introduced by flipping single spins with Metropolis transition rates

$$w(s_i \rightarrow -s_i) = \mathcal{L}^{-2} \min\{1, e^{-\Delta E/T}\}, \quad (3)$$

where ΔE is the change in energy due to the spin flip to be attempted and we have set to unity the Boltzmann constant. Time is measured in Monte Carlo steps, each of which corresponds to \mathcal{L}^2 elementary spin-flip attempts. We consider a quenching protocol where the system is initialized in a configuration sorted from an infinite-temperature equilibrium ensemble, i.e., spins are randomly and independently set to $+1$ or -1 . This initial state is evolved at the quench temperature T by means of the transition probabilities (3) with $T < T_c(\sigma)$.

Since the spin-spin interaction is long ranged, the calculation of ΔE at every spin-flip attempt via Metropolis probability (3) is computationally expensive. To speed up the computer simulation, we store the local field for each spin at the beginning of the simulation. In this way we need to update it only once the spin flip is accepted. This simple trick significantly speeds up the numerical calculations at any given quench temperature [13,25].

The main issue during the simulations of the system with Hamiltonian (1) is the strong finite-size effect arising due to the long-range character of $J(r)$. One obvious way to diminish these effects is to use periodic boundary conditions via minimum-image convention [26]. In this approach, the square lattice is mapped onto a torus where each spin in the system interacts with other spins up to a certain cutoff distance (less than or equal to $\mathcal{L}/2$). When the interaction decays slowly, this natural cutoff limit on the interaction-range causes artifacts in the simulation results. Therefore, we need a more sophisticated approach to implement periodic boundary conditions in such systems. For this, we envision an infinite two-dimensional lattice partitioned into infinite imaginary copies of the original simulation lattice. The central cell of this infinite lattice is the simulation lattice itself, and the imaginary copies, called images, lie across its periodic boundaries in both the x and y directions. Implementing periodic boundary conditions with infinite images remove cutoff errors in the simulation results of long-range interacting systems. The effective interaction between two spins inside the simulation lattice can now be expressed as an infinite summation over all images

$$J(s_i, s_j) = \sum_{n_x} \sum_{n_y} \frac{1}{|\vec{n} + \vec{r}_i - \vec{r}_j|^{2+\sigma}}, \quad (4)$$

where displacement vector $\vec{n} = (n_x, n_y)$ with $n_x, n_y = 0, \pm\mathcal{L}, \pm 2\mathcal{L}, \dots$, representing the coordinates of image systems and the simulation lattice is located at $\vec{n} = (0, 0)$. The infinite summation involved in (4) has slow convergence in coordinate space; therefore, it is difficult to handle it directly during the numerical simulations. We have adapted the Ewald summation technique [24,26,27], which uses a clever trick to

split it into two independent rapidly convergent summations, one in coordinate space and another in reciprocal space (see the Appendix).

The main observable we consider in this paper is the characteristic size of the growing domains, which we extract from the time-dependent spin configurations by means of the equal time correlation function

$$C(r, t) = \langle s_i(t) s_{i+\vec{r}}(t) \rangle, \quad (5)$$

where $\langle \dots \rangle$ is an off-equilibrium average, namely, taken over different initial conditions and thermal histories. If dynamical scaling holds, in quenches below T_c this quantity depends on a single variable as [1–5]

$$C(r, t) = f\left(\frac{r}{L(t)}\right), \quad (6)$$

where f is a scaling function and $L(t)$ has the meaning of the size of the growing domains at time t . This quantity can be extracted from the correlation function itself as [13,28,29]

$$C(r = L(t), t) = \frac{C(0, t)}{2} \equiv \frac{1}{2}. \quad (7)$$

The growth law after a quench to $T > 0$ was predicted in [12] by Bray and Rutenberg to be characterized by $z = z_{\text{CD}} = 2$ for $\sigma > 1$ and by $z = z_{\text{adv}} = 1 + \sigma$ for $\sigma \leq 1$, with logarithmic corrections at $\sigma = 1$. Such a prediction was obtained by using a continuum model, based on a Ginzburg-Landau free energy, assuming a dynamical scaling symmetry and resorting to an energy scaling argument. These results have been confirmed recently by Christiansen *et al.* [13] by means of numerical simulations of the model considered in the present paper.

In order to study the growth law $L(t)$ it is useful to consider the effective exponent $z_{\text{eff}}(t)$ defined by $1/z_{\text{eff}}(t) = d \ln L(t) / d \ln t$. Since, in order to speed our simulations, observable quantities are computed only at discrete times t_i (equally spaced in $\ln t$), the effective exponent is computed as

$$1/z_{\text{eff}}(t_i) = \frac{\ln L(t_i) - \ln L(t_{i-1})}{\ln t_i - \ln t_{i-1}}. \quad (8)$$

The effective exponent computed by means of the definition (8) may have a noisy character; therefore, we will also use the determination based on the symmetric derivative, which amounts to

$$1/z_{\text{eff}}^{(s)}(t_i) = \frac{\ln L(t_{i+1}) - \ln L(t_{i-1})}{\ln(t_{i+1}) - \ln(t_{i-1})}. \quad (9)$$

III. NUMERICAL RESULTS

Let us now discuss the outcomes of our numerical simulations. First, as a benchmark, we show in Fig. 2 the results for quenches to relatively high T , where we expect to recover results similar to those found by Christiansen *et al.* [13], thus confirming the Bray-Rutenberg asymptotic exponents. In this figure we see that an algebraic growth of $L(t)$ sets in at times $t \gtrsim 10$, for all σ values. The value of z matches with the prediction of Bray and Rutenberg, as it can be appreciated in the main figure and in the inset, where the effective exponent $1/z_{\text{eff}}$ is plotted against $L(t)$.

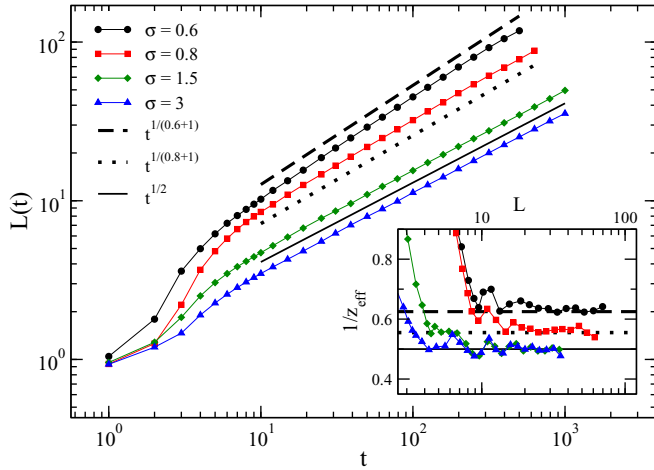


FIG. 2. Plot of $L(t)$ against t on a double logarithmic scale for systems with various values of σ (see legend) quenched from infinite temperature to final temperatures $T = 1.255, 2.929, 1.5$, and 0.9 for $\sigma = 0.6, 0.8, 1.5$, and 3 , respectively (such temperatures are in the range $0.1T_c - 0.3T_c$). The system size is 2048^2 and each data set is averaged over 10 realizations. The different lines (see legend) represent the expected asymptotic behavior $L(t) \sim t^{1/z}$, with $z = 1 + \sigma$ for $\sigma \leq 1$ and $z = 2$ for $\sigma > 1$. In the inset the effective exponent $1/z_{\text{eff}}$ is plotted against $L(t)$ on a log-linear scale. The horizontal dashed, dotted, and solid lines are the expected asymptotic values.

Let us now move to the core results of this article, namely, the effect of quenching to $T = 0$. In Fig. 3 we summarize the behavior of $L(t)$ not only in zero-temperature quenches, but also in deep quenches to small but finite T , in order to appreciate the existence of preasymptotic effects. Let us start by discussing the case with $\sigma = 3$ [Fig. 3(d)]. Since this value of σ is rather large, one could naively expect to see a behavior akin to that of the NN model. As we know, such a naive argument is correct when applied to the shallow quenches discussed above, since for any $\sigma > 1$ one recovers the exponent $z_{\text{CD}} = 2$ of the NN case. Instead, here one observe that for $T = 0$ (black curve), for $t \gtrsim 10$ one has an algebraic increase of $L(t)$ with an exponent $1/z \simeq 0.7$, definitely larger than the one, $1/z_{\text{diff}} = 0.5$, of the corresponding quench to $T = 0$ in the model with NN interactions (and of the one $1/z_{\text{CD}} = 0.5$ predicted by Bray-Rutenberg for quenches to $T > 0$ with $\sigma > 1$). Although a precise determination of z is not possible from these simulations, this is surely enough to establish the existence of a different exponent, which we denote by \mathcal{Z} , associated with the zero-temperature quenches with long-range interactions. Note that the decrease of such an exponent at large $L(t)$ (meaning very large times) must be attributed to finite-size effects.

Figure 3(d) also shows that a quench to $T = 10^{-4}$ behaves very similarly to the case with $T = 0$, whereas a quench to $T = 10^{-2}$ does so only up to times smaller than $t \simeq 10^2$, after which $L(t)$ slows down gradually until being compatible with $1/z_{\text{eff}} = 1/z_{\text{CD}} = 1/2$. This pattern of behaviors can be interpreted as a crossover occurring at $L_{\text{cross}}(T, \sigma)$ between an early regime with $z = \mathcal{Z}$ and a late stage with the Bray-Rutenberg exponent. Since $L_{\text{cross}}(T, \sigma)$ is a decreasing function of T , the crossover cannot be observed in the quench

to $T = 10^{-4}$ because it occurs after the longest simulated times.

Moving now to the other values of σ considered in Fig. 3, we observe a similar pattern of $L(t)$, with a regime characterized by a value of $1/z$ of order 0.7. This value, with the precision of our numerical simulations, appears to be roughly independent of σ , a fact that suggests that \mathcal{Z} is a universal exponent. This can be better appreciated in Fig. 4(a), where we compare $1/z_{\text{eff}}$ and $1/z_{\text{eff}}^{(s)}$ in zero-temperature quenches with various σ . This figure shows that $1/z_{\text{eff}}$ is set to a value of order $1/z_{\text{eff}} \simeq 2/3$ for $L(t)$ around $L(t) = 10$ and then slowly increases towards a value that exceeds 0.7, before bending down due to finite-size effects. A similar behavior, somewhat less noisy, is displayed by $1/z_{\text{eff}}^{(s)}$. This observation, together with the study of single-domain models that we will discuss in Sec. IV, leads us to the conjecture that the exponent \mathcal{Z} toggles between a preasymptotic value $\mathcal{Z} = 3/2$ and an asymptotic one $\mathcal{Z} = 4/3$. These two values are indicated by straight lines in Figs. 3 and 4.

Comparing the various panels of Fig. 3, one can also be convinced that the crossover length $L_{\text{cross}}(T, \sigma)$ is a (rather strongly) decreasing function of σ . Indeed, for instance, with $\sigma = 0.9$ [Fig. 3(c)], one has to increase T by a factor 10^2 (i.e., to set $T = 1$) in order to see a crossover pattern similar to the one observed at $\sigma = 3$ (at $T = 10^{-2}$). Moreover, one observes that finite-size effects are more important for the smaller values of σ because the longest range of the interactions makes the system experience the periodic boundary conditions earlier.

Finally, let us discuss the issue of dynamical scaling. This was shown to be obeyed [13] in the Bray-Rutenberg regime occurring in quenches to a finite T , by checking the form (6) of the correlation function. In the following we study the same matter in the zero-temperature quenches. Our results for $C(r, t)$ are shown in Fig. 5. The data for different times show a very good collapse when plotted against the rescaled variable $r/L(t)$, as expected after Eq. (6) in the presence of dynamical symmetry. This is true for all the values of σ considered (we show only a couple of them in Fig. 5, but similar results are found for the other values). For $\sigma = 0.8$ [Fig. 5(a)], the curve at the longest time $t = 500$ starts departing from the collapse, but this is due to the onset of finite-size effects which can also be detected at these times from the behavior of $L(t)$ shown in Fig. 3. Hence, we conclude that the dynamical scaling symmetry is at work also in zero-temperature quenches, a fact that will be used in the following. Let us also mention that metastable states, which are very important with NN interactions, here are absent (or at least greatly suppressed), as found also in [30].

IV. EVOLUTION OF A SINGLE DOMAIN

In the preceding section we have shown that, with long-range interactions, one observes a fast growth regime at $T = 0$ regulated by an exponent $1/\mathcal{Z} \simeq 0.7$. However, in the absence of analytic approaches or of a detailed comprehension of the mechanism at work, a precise determination of such an exponent on the basis of the sole simulations could not be obtained.

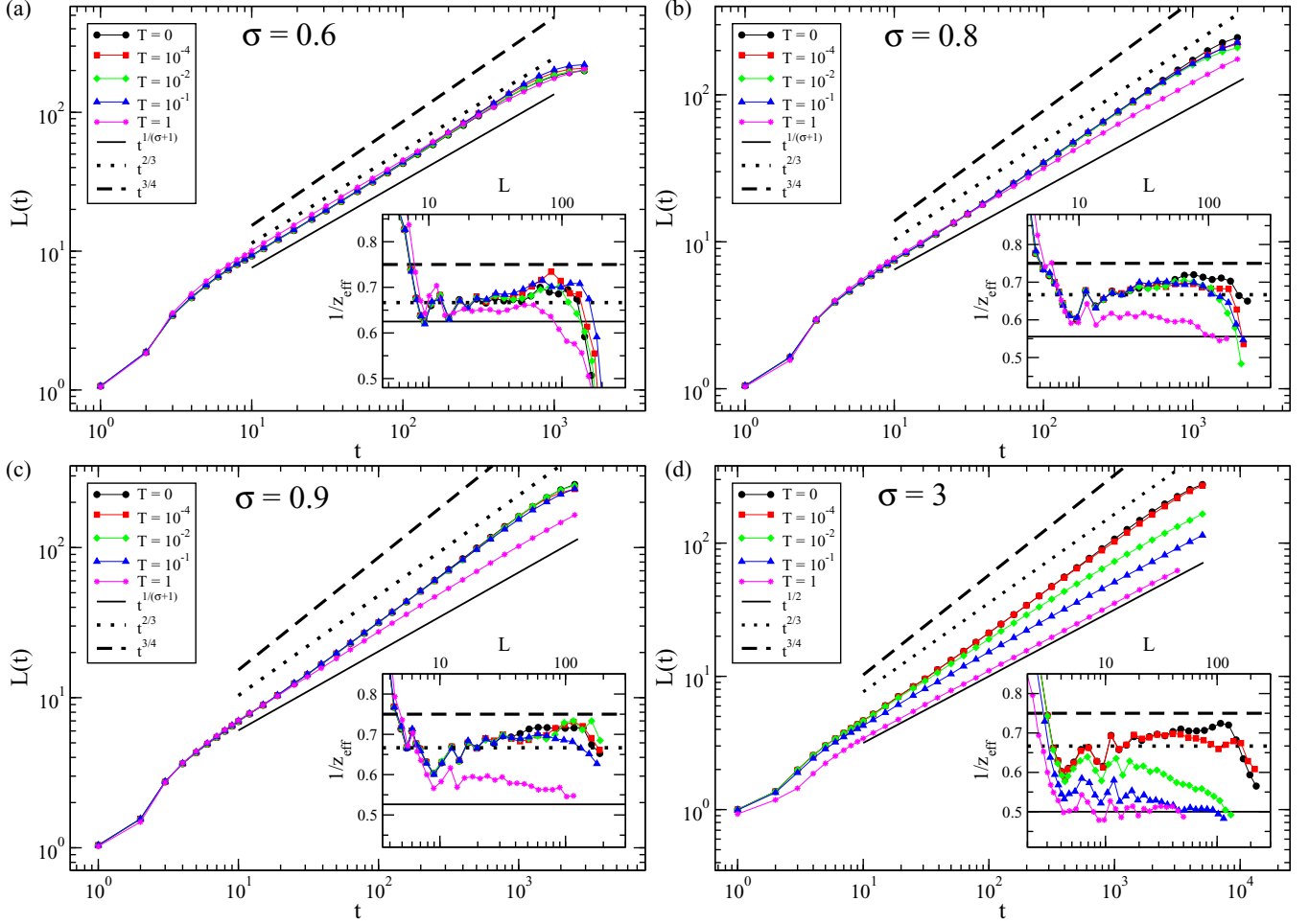


FIG. 3. Plot of $L(t)$ against t on a double logarithmic scale for systems with various values of σ (see legends) quenched from infinite temperature to different final temperatures (see legends). The system size is 2048^2 and each data set is averaged over 40 realizations. The solid, dotted, and dashed lines (see legends) represent the expected asymptotic behavior at finite temperatures and the two putative behaviors $t^{2/3}$ and $t^{3/4}$ expected preasymptotically and at late times at zero and low temperatures. In the inset the effective exponent $1/z_{\text{eff}}$ is plotted against $L(t)$ on a log-linear scale. The horizontal solid, dashed, and dotted lines are the above-discussed expected asymptotic and preasymptotic exponents.

In this section we study the simpler process with a single domain. This approach has been shown to provide a correct determination of the growth exponent z in systems with NN interactions, for any d [11,31,32], and also with long-range interactions in $d = 1$ [16]. We consider the same model of Sec. II with the only difference that the initial state is not sorted from an infinite-temperature ensemble but is built by hand with a single domain of size R . This configuration is evolved with the flip probabilities (3), which lead to a shrinkage and eventual disappearance of the bubble. We start with a circular shape of radius R (more precisely, the lattice approximation to a circle, as in Fig. 6), because we observed that, starting from different shapes, a roughly circular one tends to be formed during the evolution after a transient (however, the true asymptotic shape is not perfectly circular; see the discussion in Sec. IV C). This is shown in Fig. 7 for an initially square bubble. Notice that the late geometry of the bubble is almost isotropic, at variance with what was observed with the NN interaction during coarsening [33] or in metastable states [34]. The idea behind this single-domain approach is based on the dynamical scaling hypothesis which simply means that

at any time t in a coarsening system there is only a relevant length $L(t)$. According to this assumption, the average time $t(L)$ needed to close a domain of initial size L in such a system scales as L^z . Here we adopt the stratagem is to compute $t(L)$ with a single domain. Since R is the initial size of such a domain, we indicate with $t(R)$ this quantity and use $t(R) \sim R^z$ as a proxy for $t(L)$. This of course implies another assumption, namely, that the shrinkage of a domain is not significantly influenced by the presence of the others, so a single-domain configuration suffices. Previous studies [11,16,31,32] proved that such an approach works well because as long as $\sigma > 0$ the interaction is integrable, i.e., $\sum_r J(r)$ is finite. This means that the interaction between spins at distance larger than L , in the asymptotic stage when L has grown large, is negligible.

A. Numerical results

To start with, we have implemented numerical simulations of the bubble shrinkage process and we have computed $t(R)$ by averaging over many dynamical trajectories. The results are contained in Fig. 8, where in each panel we plot $t(R)$ (on

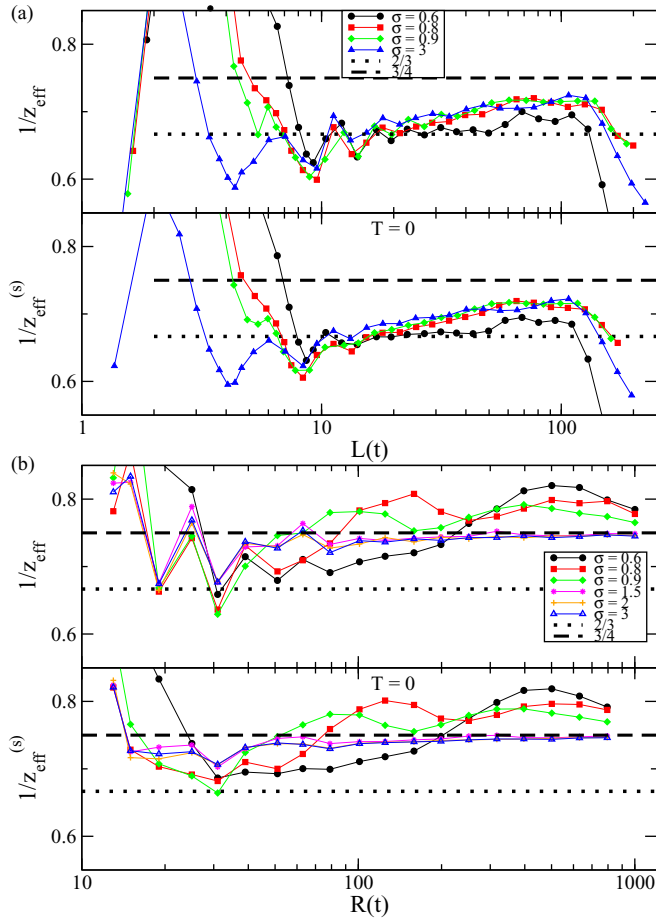


FIG. 4. Comparison between the effective exponents $1/z_{\text{eff}}$ and $1/z_{\text{eff}}^{(s)}$ in the quench to $T = 0$ with various values of σ presented on a log-linear scale. (a) Same data as in Fig. 3 for the coarsening multidomain system (only for $T = 0$). (b) Same data as in Fig. 8 for the single shrinking bubble model. The dashed and dotted lines are the values $3/4$ and $2/3$, respectively.

the x axis) vs R (on the y axis). This choice allows us a direct comparison with Fig. 3, where we plotted $L(t)$ versus t for an extended multidomain system. For the same reason we also

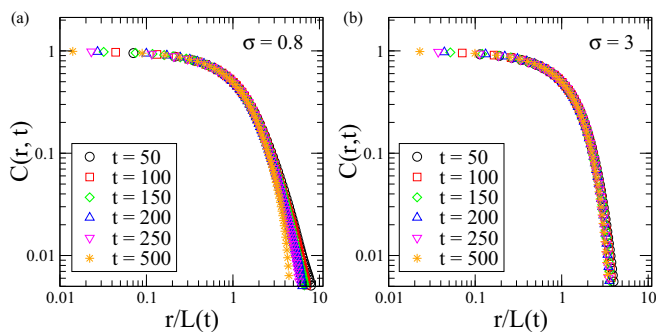


FIG. 5. Plot of $C(r,t)$ against $r/L(t)$ on a double logarithmic scale for systems with (a) $\sigma = 0.8$ and (b) $\sigma = 3$ quenched from infinite to zero temperature. Different symbols and colors refer to different times, as shown in the legend. The system size is 2048^2 and each data set is averaged over 40 realizations.

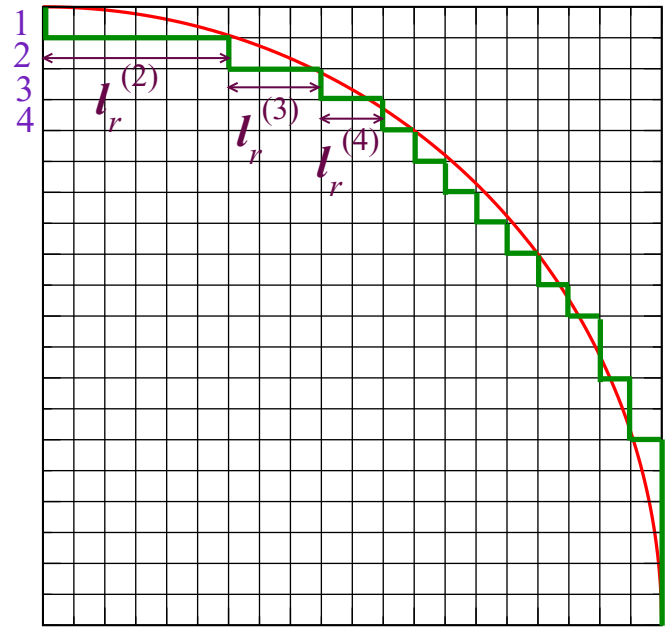


FIG. 6. Pictorial representation of a circular domain (only one quadrant) on a square lattice. Spins are located in the center of the small squares forming the lattice. The domain can be viewed as the superposition of terraces, numbered according to the violet figures near the vertical axis. The droplet is shown at a time when the upper terrace (number 1) has shrunk to zero and is disappearing. In this configuration the length of the j th terrace is indicated with $\ell_r^{(j)}$. With the simplified dynamics described in Sec. IV C, only the edge spins can flip. The red curve is a circle in the continuum.

plot the effective exponent, defined previously in Eq. (8) (with the replacement $L \rightarrow R$), in the inset.

Let us start with the case $\sigma = 3$ [Fig. 8(f)]. Working at $T = 0$, one sees that a very clean value $1/z_{\text{eff}} = 0.75$ sets in for large R , providing $\mathcal{Z} = 4/3$. Instead, for very small sizes the effective exponent has a zigzag behavior. This is perhaps due to the fact that for such small sizes some fine geometrical details of the initial state become relevant. We notice indeed that the most pronounced peaks (local maxima) of $1/z_{\text{eff}}$ correspond to values of $R = n^2$, where n is an integer. As we will further discuss below, as shown with Eq. (11), when the bubble diameter is a perfect square number the largest terrace ℓ_L of the domain (the horizontal segment denoted by 1 in Fig. 6) is naturally an integer, thus determining a discontinuity in the dynamical process. This effect clearly reduces and tends to disappear with increasing R . If we neglect these special maxima, for small R the effective exponent hits twice the value $1/z_{\text{eff}} = 2/3$. This might suggest that \mathcal{Z} toggles between a preasymptotic value $\mathcal{Z} = 3/2$ and an asymptotic one $\mathcal{Z} = 4/3$. This conjecture is going to be further supported. The asymptotic value $4/3$ is assumed for $R \gtrsim 10^2$. Comparing with the coarsening data of Fig. 3, we can conclude that domains of such sizes are only reached at the very end of the coarsening simulation when finite-size effects start to set in. This would explain why in the coarsening simulations one mostly observes an exponent in between $\mathcal{Z} = 3/2$ and $\mathcal{Z} = 4/3$ and only a hint of the convergence to the late one $\mathcal{Z} = 4/3$ can be observed. Looking now still in Fig. 8 for $\sigma = 3$ but

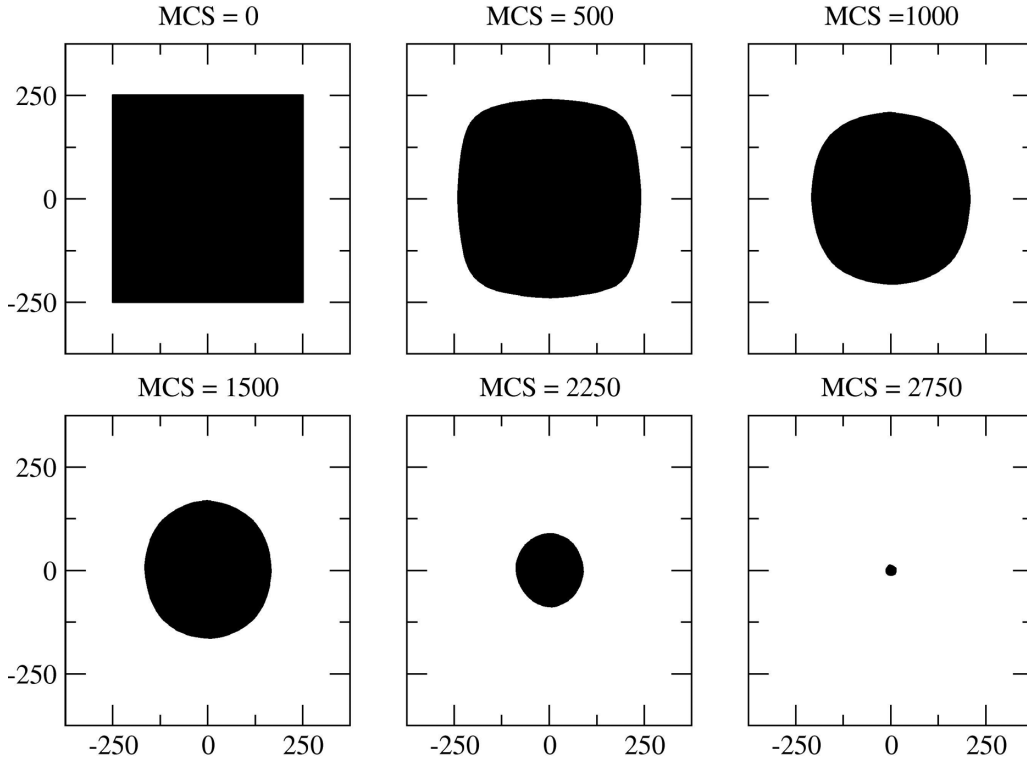


FIG. 7. Shrinkage of an initially square bubble of size 500 shown for $T = 0$ and $\sigma = 3$. Different snapshots correspond to the simulation times reported on top of the panels [times are expressed in Monte Carlo steps (MCS)].

focusing on the data at the finite temperature $T = 0.5$, one sees that the effective exponent attains the value of Bray and Rutenberg, $1/z = 0.5$. This result attests to the correctness of the single-domain configuration to extract the exponent z .

We can now pass to the other panels of Fig. 8, corresponding to smaller values of σ . At finite T one concludes that there is a crossover phenomenon at a value $R_{\text{cross}}(T, \sigma)$, where the exponent z changes from \mathcal{Z} to the Bray and Rutenberg value [for $\sigma = 0.6$, $R_{\text{cross}}(T, \sigma)$ is probably too large to observe the crossover]. At $T = 0$ the same value $\mathcal{Z} = 4/3$ is neatly observed also for $\sigma = 1.5$ and 2. For values of σ smaller than one, the determination of such an exponent turns out to be less precise and there is the tendency to observe larger values of $1/z_{\text{eff}}$ upon decreasing σ . This could be due to a stability effect that we will discuss below. The data for the effective exponent at $T = 0$ are summarized in Fig. 4(b).

B. Stability of the bubble

After having presented the results of the simulations of the bubble shrinkage, which provide a determination of the growth law in a semiquantitative agreement with what was observed in the full coarsening model, we turn now to a study of the microscopic kinetic mechanisms producing the closure process, in order to gain a better understanding. We start by discussing the stability properties of an interface between two regions with differently aligned spins. The zero- T stability of a (positive, say) spin depends on the total field h acting on it. If $h > 0$ the spin is stable (meaning that it cannot flip), if $h < 0$ the spin is unstable, and if $h = 0$ the spin can also flip

but this usually corresponds to a neutral equilibrium, typical of the NN model (discussed below) but not of the long-range one, because a perfect compensation of extended interactions leading to $h = 0$ is almost impossible.

In Fig. 1 we consider different types of discrete interfaces and we refer the reader to its detailed caption. A straight interface parallel to a lattice axis [see Fig. 1(a)] is clearly stable because all spins parallel to a given interface spin, denoted by a closed black circle, block its reversal while all other spins, above and below such a line, perfectly compensate. This is true for long-range coupling but also for NN coupling: In the former case all closed gray circles block the closed black circles, in the latter case only its two neighboring ones. When the interface contains kinks, either keeping a constant slope (i.e., all the steps have the same length) as in Fig. 1(b) or acquiring a finite curvature as in Figs. 1(c) and 1(d), things are different and more complicated. In the NN case kinks do not interact and each of them can move in both directions even at $T = 0$. With long-range interactions the picture is completely different and we must distinguish between the two sides of the kink. Let us always focus on the closed-black-circle spins. If the interface has a constant slope it is stable; this is shown in Fig. 1(b) (see the discussion in the caption). Notice that this is true irrespectively of the value of σ . If the interface has a finite curvature as in Fig. 1(c), the closed-black-circle spin is unstable while the spin at its right is stable, meaning that the kink can move uphill (to the left) only. This also occurs for any σ . In Fig. 1(d) the interface has a constant slope locally around the closed black circle, i.e., terraces locally have the same length, but further uphill and downhill terraces are longer

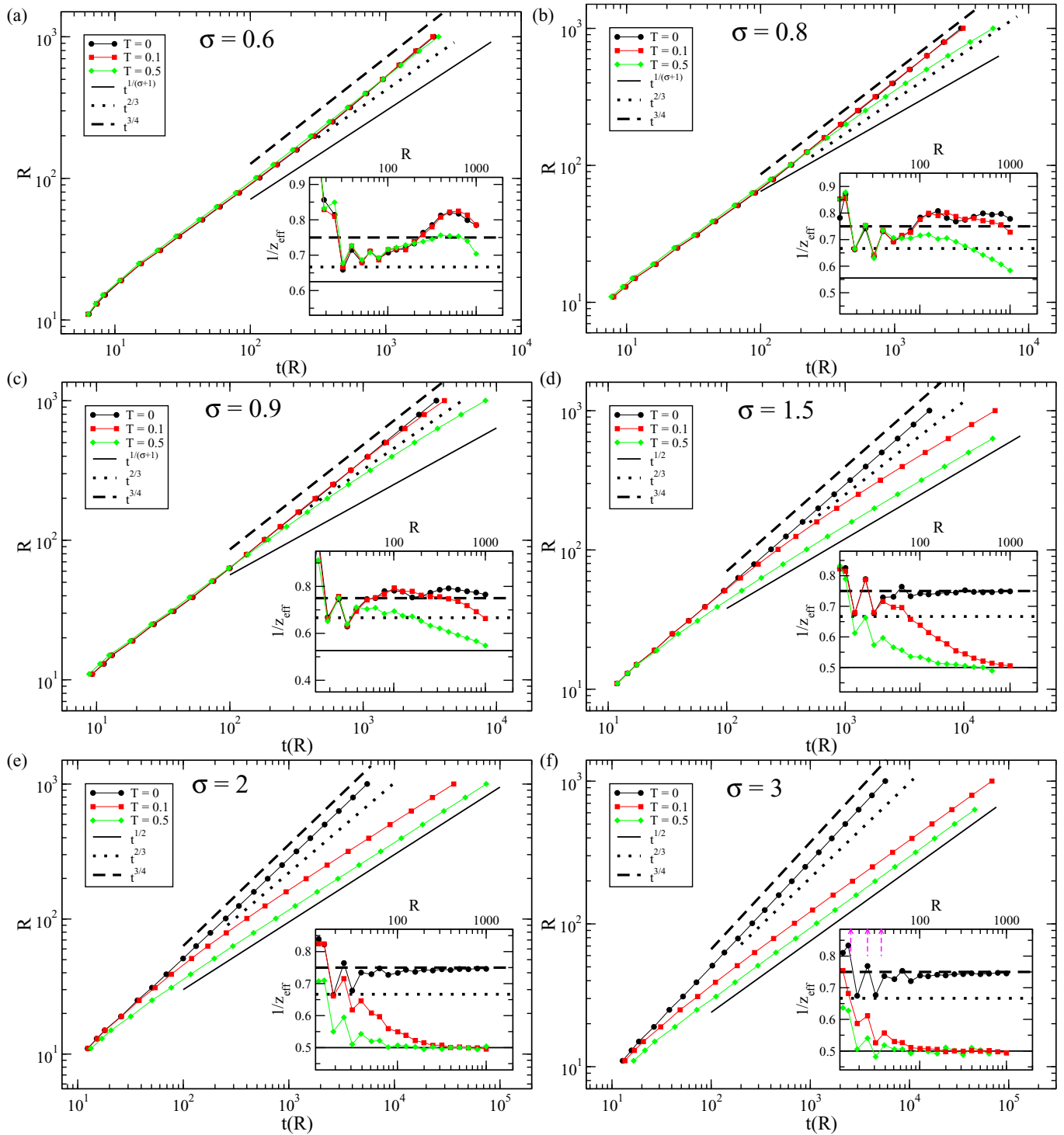


FIG. 8. Closure time $t(R)$ of an initially circular bubble of diameter R (on the x axis) plotted against R (y axis) on a double logarithmic scale for different temperatures (see legends) and different values of σ : (a) $\sigma = 0.6$, (b) $\sigma = 0.8$, (c) $\sigma = 0.9$, (d) $\sigma = 1.5$, (e) $\sigma = 2$, and (f) $\sigma = 3$. The system size is 2048^2 . Data are averaged over 10^3 realizations for $R \leq 100$ and over 10 – 10^2 realizations for larger values of R . The dotted and dashed lines represent the two putative behaviors $t^{2/3}$ and $t^{3/4}$ expected preasymptotically and at late times at low temperatures, respectively. In the inset the effective exponent $1/z_{\text{eff}}$ is plotted against R on a log-linear scale. The horizontal solid, dashed, and dotted lines are the expected asymptotic and preasymptotic exponents. The dashed magenta upward arrows in (f) indicate the first three values of R such that \sqrt{R} is an integer (see the text), namely, $R = 16, 25, 36$.

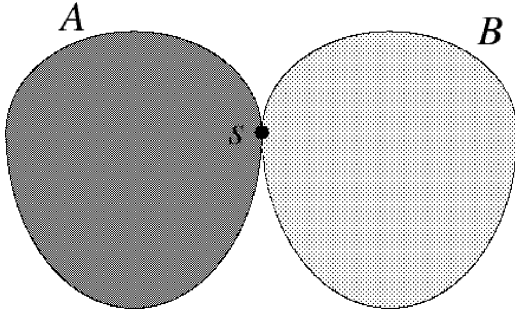


FIG. 9. Here A (dark gray) is a general compact (negative) domain in a sea of positive spins. At any point of its surface (where spin s is located) we can imagine drawing the mirror domain B (light gray) tangent to it. For symmetry reasons the field produced by the negative domain A on spin s is exactly compensated by the field produced by the positive domain B , leaving the remaining white region, which is positively magnetized and which therefore induces a constant drift favoring the closure of domain A .

and shorter, respectively. In this case there are short-distance stabilizing interactions (due to parallel uncompensated spins) and longer-distance destabilizing interactions (due to antiparallel uncompensated spins). The global effect depends on the details of the interface and on the value of σ ; it is likely that stability prevails for large σ and instability prevails for small σ . Finally, in Fig. 1(e) it is shown that also the edge spins of a top terrace are unstable.

Things are even more complicated when considering interface spins not at a kink. As a matter of fact, in the limit of small σ , even bulk spins can flip. In particular, considering a circular domain of size R , the central spin is unstable up to a critical size $R = R_c \sim 2^{1/\sigma}$. Indeed, the spin cannot flip when the stabilizing interaction of order $\int_{r < R} d\vec{r} r^{-(2+\sigma)}$ prevails over the destabilizing one of order $\int_{r > R} d\vec{r} r^{-(2+\sigma)}$ produced by the antialigned spins outside the domain, which gives the above-mentioned result. Note that in our bubble shrinkage simulations, in order to have a reliable asymptotic (i.e., large R) determination of $t(R)$ one has to consider $R \gg R_c$; otherwise there is a correction lowering $t(R)$ (because the domain shrinks to zero almost immediately as soon as R crosses R_c). Since for $\sigma \rightarrow 0$ it is $R_c \rightarrow \infty$, this is the possible explanation of the observation made, regarding Fig. 8, that decreasing σ , one observes values of $1/\mathcal{Z}$ larger than $3/4$. In Sec. IV C we will clearly show the role of bulk spin flips.

We conclude this section by stressing that our results are strongly related to the discreteness of the lattice. In a continuum medium any surface spin of a compact bubble would experience a field favoring the closure of the bubble itself (see Fig. 9) because the field produced by spins within the bubble is always compensated by the field due to the mirror domain. Uncompensated spins are antiparallel to bubble spins, thus inducing its closure. At zero temperature this uniform driving force would give a trivial dynamical exponent $z = 1$.

C. Simplified dynamics and determination of \mathcal{Z}

In Sec. IV B we discussed at a semiquantitative level the role of bulk spin flips which produce finite-size effects whose importance increases with decreasing σ . The behavior of

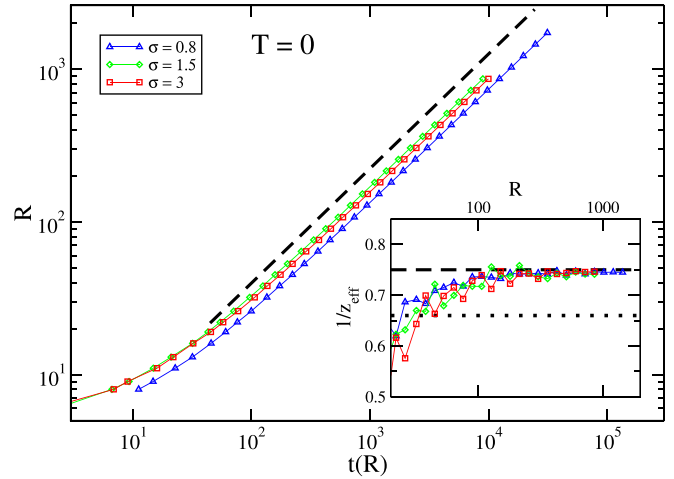


FIG. 10. Closure time $t(R)$ of a bubble of size R (on the x axis) plotted against R (y axis) on a double logarithmic scale, at $T = 0$ and using the simplified dynamics where only corner spins can flip. Data are averaged over 100 realizations. The dashed line represents the behavior $t^{3/4}$. In the inset the effective exponent $1/z_{\text{eff}}$ is plotted against R on a log-linear scale. The horizontal dotted and dashed lines are the expected preasymptotic and asymptotic exponents $2/3$ and $3/4$, respectively.

interfacial spins with three aligned neighbors and the fourth pointing in the opposite direction (namely, spins on a locally flat interface) is more difficult to investigate. However, we can imagine that, at least at a qualitative level, they should behave similarly to the bulk ones, in that they are stable for large σ and bubble sizes R and become unstable upon decreasing R , particularly for small σ . According to this reasoning, these spins together with the bulk ones introduce finite-bubble-size effects that are more severe for small values of σ . As already mentioned, we believe these finite-size effects to be responsible for the effective exponent z_{eff} somewhat larger than $4/3$ observed for small σ in Fig. 8 and in Fig. 4(b). In order to avoid them, here we offer simulations where flips in the bulk and with three aligned neighbors are forbidden.

Results of simulations conducted with this simplified dynamics at $T = 0$ are shown in Fig. 10. Our data clearly prove that the dynamical exponent with the simplified dynamics is $\mathcal{Z} = 4/3$ for all σ . This suggests that this exponent is universal (i.e., independent of σ) and that $4/3$ is its truly asymptotic value. However, according to the previous considerations, in order to see this value with comparable evidence for small σ in full simulations one should access very large bubble sizes, which is not feasible with our current numerical resources.

In order to clarify the physical mechanisms leading to $\mathcal{Z} = 4/3$ and to the preasymptotic value $\mathcal{Z} = 3/2$, it is necessary to have a more detailed study of the shape of the shrinking bubble. If we focus on a quadrant and suppose that only edge spins can flip, the dynamics of the droplet can be reduced to that of the terraces pictorially depicted in Fig. 6. We indicate with $l_r^{(j)}$ the length of the j th terrace exactly at the time step when the top terrace shrinks to zero, in the configuration when the bubble radius is (at that time) r .

Taking into account that the kink on the upper terrace always moves ballistically, we find that the time necessary for

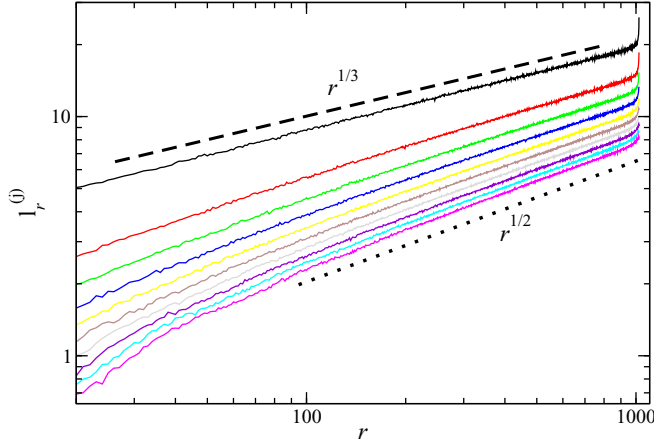


FIG. 11. Length of the j th terrace $\ell_r^{(j)}$ at the closure time of the top terrace plotted against r , for $j = 1-10$, from top to bottom. The dashed line is the power law $r^{1/3}$, whereas the dotted line is the power law $r^{1/2}$.

the droplet to disappear is

$$t(R) = \sum_{r=2}^R \ell_r^{(2)} + \ell_R, \quad (10)$$

where ℓ_R is the length of the top terrace in the initial configuration. The evaluation of $\ell_r^{(2)}$ is complicated because of the “long-range” interaction between terraces. An analytical expression for $\ell_r^{(2)}$ can be obtained from the observation (see Fig. 7) that, independently of the initial configuration, the droplet asymptotically assumes a quasicircular shape. Assuming that the droplet is *exactly* circular at all times, the quantity $\ell_r^{(2)}$ is obtained from the equation of the boundary in the continuum, $x^2 + y^2 = r^2$, as the value of x corresponding to $y = r - 1$,

$$\ell_r^{(2)} = \sqrt{2r - 1} \simeq \sqrt{2r}. \quad (11)$$

Inserting this expression in Eq. (10), we get $t(R) \sim R^{3/2}$, hence $\mathcal{Z} = 3/2$. This value, as we know, is observed for small R , whereas for large R it crosses over to $\mathcal{Z} = 4/3$, indicating a deviation from the circular profile of the upper terraces. This deviation must be attributed to the interaction between different terraces, in particular because of the drive exerted by the ballistic upper terrace transporting to some extent the lower ones. In order to be more quantitative about this, in Fig. 11 we plot results for $\ell_r^{(j)}$ as a function of r for $j \leq 10$. Let us look at the region $10^2 < r < 10^3$. In this sector one sees that the size of the innermost terrace considered, namely, $j = 10$ (lowest curve, magenta), grows as $r^{1/2}$. Recalling Eq. (11) and observing that also $\ell_r^{(j)} \propto \sqrt{r}$ for $r \gg j$, this is what one would expect for a circular domain indicating that, sufficiently far from the top of the domain, its shape is circular. However, upon decreasing j , that is, considering higher terraces, this slope gradually decreases until, for $j = 2$, the top terrace behaves as $\ell_r^{(2)} \sim r^{1/3}$. Using this result in Eq. (10), one gets from the behavior of this terrace the correct asymptotic value $\mathcal{Z} = 4/3$. This shows that the origin of this number must be traced back to the nontrivial geometry of the domains induced by nonlocal interactions between terraces. The actual

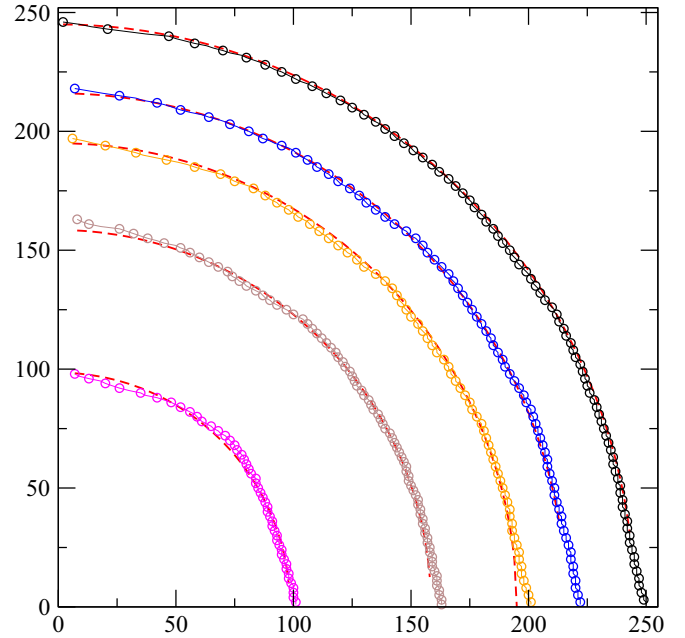


FIG. 12. Shape of the shrinking bubble with the approximated dynamics for $\sigma = 0.8$. Different symbols corresponds to the droplet configuration at different times $t = 10 \times 2^i$, with $i = 1, 4, 5, 6$ increasing from top to bottom. The dashed red curve is a circle in the continuum.

shape of the domain during its shrinkage is shown in Fig. 12, where one can see deviations from circularity in the top and rightmost part of the bubble. Notice that such deviations are hardly visible to the naked eye; however, their effect on \mathcal{Z} is important enough to change its value from $3/2$ to $4/3$.

To complete the discussion of Fig. 11, let us note that there is a steep increase at $r \gtrsim 10^3$ and also that the algebraic behavior of the curves is spoiled for small values of r . The former effect is due to the fact that the simulation is initialized with a domain of size greater than or approximately 1000 and it takes some time for the dynamical process to build the domain’s shape and to enter the scaling stage. The latter effect occurs because, in the very late stage of the process when the domain is very small, the scaling properties are lost because there are not enough interacting terraces to produce a many-body phenomenon.

V. CONCLUSION

In this paper we have shown that during the zero-temperature relaxation dynamics of the two-dimensional long-range Ising model a new dynamical regime appears, which is characterized by an exponent \mathcal{Z} that takes a preasymptotic value $\mathcal{Z} = 3/2$ and an asymptotic one $\mathcal{Z} = 4/3$. These values are strongly related to the interplay between the discrete nature of the lattice and the long-range nature of the interaction. In fact, if interactions are short ranged (NN model) we would have $z_{\text{CD}} = 2$ both in a discrete lattice and in a continuum picture (see Sec. I). On the other hand, a continuum picture with long-range interactions would trivially give $z = 1$ (see Fig. 9 and related discussion at the end of Sec. IV B).

The preasymptotic value $\mathcal{Z} = 3/2$ [see Eqs. (10) and (11)] is simply understandable. For this, we use a discrete approximation of a circular bubble and assume that its shrinkage dynamics is limited by the closure of the largest terraces. However, Fig. 11 shows that the largest terraces scale as $r^{1/3}$ rather than as $r^{1/2}$, as expected for a circular bubble. This results in the true asymptotic value $\mathcal{Z} = 4/3$. The reason for such a behavior (see Sec. IV C) can be associated with the long-range character of the interaction and the necessity to locally preserve a convex shape of the bubble in order for the dynamics to proceed. Apart from this phenomenological understanding of the mechanism producing the asymptotic value $\mathcal{Z} = 4/3$, a rigorous analytical derivation has not yet been possible.

Given the paucity of analytic approaches, further analysis is confined to better numerical simulations of the multidomain system. To be useful, these must go beyond the timescales and the statistical accuracy of those presented in this paper. As we estimate below, this seems to be possible, but entails a huge computational effort. Figure 4 shows that the effective exponent would reasonably approach the value $4/3$ for sizes of order $L(t) \simeq 200$ – 300 . Thus, one should check for its further behavior up to, say, $L(t) \simeq 500$ – 600 . Figure 3 informs us that, in order to reach this point, we should go to times of order $t \simeq 10^4$. Also, from the same figure one understands that finite-size effects start to be important around $L(t) \simeq 100 \simeq \mathcal{L}/20$. Hence, in order to reach $L(t) \simeq 500$ without severe finite-size effects, the system should have at least a size $\mathcal{L} \simeq 10^4$. Putting the above facts together, we estimate a required computational effort at least 100 times larger than the one of this study, which is already quite massive. This estimate applies for the larger values of σ ; for smaller values the situation is much worse.

The study of this paper is restricted to a two-dimensional square lattice. However, since we have emphasized that lattice effects are relevant in determining the $T = 0$ growth exponent, an interesting question to be still addressed is the universality of the exponent \mathcal{Z} with respect to the lattice geometry. In this direction, numerical simulations of $d = 2$ systems on different lattices (e.g., triangular or hexagonal lattices) would be useful. Similarly, the dependence on

dimensionality should also be considered, although the numerical effort required would be further increased. Finally, the dynamics with extremely long-range interactions (i.e., with $\sigma \leq 0$) remains a completely unexplored subject in any dimension.

Note added. Recently, Christiansen *et al.* [30] also found the exponent $3/4$ independently of σ .

ACKNOWLEDGMENT

E.L. and P.P. acknowledge support from the MIUR PRIN Project No. 201798CZLJ.

APPENDIX: EWALD SUMMATION TECHNIQUE

Combining the effective interaction between two spins described by Eq. (4) in Eq. (1), the Hamiltonian for the long-range Ising model takes the form

$$\mathcal{H}(\{s_i\}) = -\frac{1}{2} \sum_{\vec{n}} \sum_i \sum_j \frac{1}{|\vec{n} + \vec{r}_{ij}|^{2+\sigma}} s_i s_j, \quad (\text{A1})$$

where $\vec{r}_{ij} = \vec{r}_i - \vec{r}_j$ and the summation over \vec{n} accounts for the contribution of infinite imaginary copies across periodic boundaries. The prime in this summation indicates that, when $\vec{n} = (0, 0)$, the terms with $i = j$ are excluded. In this Appendix we will split the summation over \vec{n} into a combination of two rapidly convergent summations. For this, we take the help of complete and incomplete Gamma functions defined, respectively, as

$$\Gamma(x) = \int_0^\infty t^{x-1} e^{-t} dt, \quad (\text{A2})$$

$$\Gamma(x, y) = \int_y^\infty t^{x-1} e^{-t} dt. \quad (\text{A3})$$

The trick of Ewald, which was originally proposed for the Coulomb potential [26,27], is introduced as follows. First, we use the integral of Eq. (A2) and divide the interval of integration into two parts

$$\begin{aligned} J(s_i, s_j) &= \sum_{\vec{n}} \frac{1}{|\vec{n} + \vec{r}_{ij}|^{2+\sigma}} = \sum_{\vec{n}} \frac{1}{\Gamma(\sigma/2 + 1)} \int_0^\infty \frac{1}{|\vec{n} + \vec{r}_{ij}|^{2+\sigma}} t^{\sigma/2} e^{-t} dt \\ &= \sum_{\vec{n}} \frac{1}{\Gamma(\sigma/2 + 1)} \left(\int_0^{\alpha^2 |\vec{n} + \vec{r}_{ij}|^2} \frac{1}{|\vec{n} + \vec{r}_{ij}|^{2+\sigma}} t^{\sigma/2} e^{-t} dt + \int_{\alpha^2 |\vec{n} + \vec{r}_{ij}|^2}^\infty \frac{1}{|\vec{n} + \vec{r}_{ij}|^{2+\sigma}} t^{\sigma/2} e^{-t} dt \right), \\ &= I_1 + I_2, \end{aligned} \quad (\text{A4})$$

where α is a positive real number. The separated terms, denoted by I_1 and I_2 , represent the contributions of the integral over intervals $0 < t < \alpha^2 |\vec{n} + \vec{r}_{ij}|^2$ and $\alpha^2 |\vec{n} + \vec{r}_{ij}|^2 < t < \infty$, respectively.

Looking at the second term given in Eq. (A4), one can write, with the help of Eq. (A3),

$$I_2 = \frac{1}{\Gamma(\sigma/2 + 1)} \sum_{\vec{n}} \frac{1}{|\vec{n} + \vec{r}_{ij}|^{2+\sigma}} \Gamma\left(\frac{\sigma}{2} + 1, \alpha^2 |\vec{n} + \vec{r}_{ij}|^2\right). \quad (\text{A5})$$

This term rapidly converges as $|\vec{n}|$ increases, representing the short-range contribution of the exchange interaction between spins s_i and s_j .

To simplify the first term, we use the change of variables $\rho^2 |\vec{n} + \vec{r}_{ij}|^2 = t$,

$$I_1 = \frac{2}{\Gamma(\sigma/2 + 1)} \sum_{\vec{n}} \int_0^\alpha \rho^{\sigma+1} e^{-|\vec{n} + \vec{r}_{ij}|^2 \rho^2} d\rho. \quad (\text{A6})$$

The above term can also be made rapidly convergent by transforming to reciprocal space. We use the Poisson summation formula to obtain

$$\sum_{\vec{n}} e^{-|\vec{n}+\vec{r}_{ij}|^2 \rho^2} = \frac{\pi}{\mathcal{L}^2 \rho^2} \sum_{\vec{k}} e^{-\pi^2 |\vec{k}|^2 / \rho^2} e^{i2\pi \vec{k} \cdot \vec{r}_{ij}}, \quad (\text{A7})$$

where the reciprocal vector $\vec{k} = (k_x, k_y)$, with $k_x, k_y = 0, \pm 1/\mathcal{L}, \pm 2/\mathcal{L}, \dots$. As mentioned in the main text, \mathcal{L} denotes the system size. Using the expression (A7) in Eq. (A6) and recalling Eq. (A3), the first term (A6) can be written as

$$I_1 = \frac{2\pi}{\mathcal{L}^2 \Gamma(\sigma/2 + 1)} \sum_{\vec{k}} e^{i2\pi \vec{k} \cdot \vec{r}_{ij}} \frac{1}{2} (\pi |\vec{k}|)^\sigma \Gamma\left(-\frac{\sigma}{2}, \frac{\pi^2 |\vec{k}|^2}{\alpha^2}\right). \quad (\text{A8})$$

This term rapidly becomes negligible as $|\vec{k}|$ increases, representing the long-range contribution of exchange interactions. Combining Eqs. (A5) and (A8) in Eq. (A4) provides the essence of the Ewald summation technique. One should also note that the summations over \vec{n} and \vec{k} in Eqs. (A5) and (A8), respectively, are conditionally convergent, i.e., the convergence of the summations depend on the order of adding terms in the summations. The best way is to sum spherically over $|\vec{n}|$ and $|\vec{k}|$.

The auxiliary parameter α determines the speed of convergence of summations over $|\vec{n}|$ and $|\vec{k}|$. We have taken the value of $\alpha = 2/\mathcal{L}$, also chosen in recent paper [24], which allows us to truncate the summation to $|n| \leq 5\mathcal{L}$ in I_2 [Eq. (A5)] and to $|k| \geq 5/\mathcal{L}$ in I_1 [Eq. (A8)]. To calculate complete and incomplete Γ functions in the numerical simulations, we have used the FORTRAN interface of the GNU scientific library in GFORTTRAN.

-
- [1] S. Puri and V. Wadhawan, *Kinetics of Phase Transitions* (Taylor & Francis, Abingdon-on-Thames, 2009).
- [2] A. Bray, *Adv. Phys.* **43**, 357 (1994).
- [3] F. Corberi and P. Politi, *C. R. Phys.* **16**, 255 (2015).
- [4] F. Corberi, *C. R. Phys.* **16**, 332 (2015).
- [5] H. Y. F. Corberi and L. F. Cugliandolo, in *Dynamical Heterogeneities in Glasses, Colloids, and Granular Media*, edited by L. Berthier, G. Biroli, J.-P. Bouchaud, L. Cipelletti, and W. van Saarloos (Oxford University Press, Oxford, 2011).
- [6] A. Bray, *Phys. Rev. B* **41**, 6724 (1990).
- [7] R. J. Glauber, *J. Math. Phys.* **4**, 294 (1963).
- [8] S. M. Allen and J. W. Cahn, *Acta Metall.* **27**, 1085 (1979).
- [9] K. Barros, P. L. Krapivsky, and S. Redner, *Phys. Rev. E* **80**, 040101(R) (2009).
- [10] T. Blanchard, F. Corberi, L. F. Cugliandolo, and M. Picco, *Europhys. Lett.* **106**, 66001 (2014).
- [11] F. Corberi, E. Lippiello, and M. Zannetti, *Phys. Rev. E* **78**, 011109 (2008).
- [12] A. J. Bray and A. D. Rutenberg, *Phys. Rev. E* **49**, R27(R) (1994).
- [13] H. Christiansen, S. Majumder, and W. Janke, *Phys. Rev. E* **99**, 011301(R) (2019).
- [14] H. Christiansen, S. Majumder, M. Henkel, and W. Janke, *Phys. Rev. Lett.* **125**, 180601 (2020).
- [15] A. D. Rutenberg and A. J. Bray, *Phys. Rev. E* **50**, 1900 (1994).
- [16] F. Corberi, E. Lippiello, and P. Politi, *J. Stat. Phys.* **176**, 510 (2019).
- [17] F. Corberi, E. Lippiello, and P. Politi, *J. Stat. Mech.* (2019) 074002.
- [18] F. Corberi, E. Lippiello, and P. Politi, *Phys. Rev. E* **102**, 020102(R) (2020).
- [19] G. Stell, *Phys. Rev. B* **1**, 2265 (1970).
- [20] M. E. Fisher, S.-k. Ma, and B. Nickel, *Phys. Rev. Lett.* **29**, 917 (1972).
- [21] J. Sak, *Phys. Rev. B* **8**, 281 (1973).
- [22] E. Luijten and H. W. J. Blöte, *Phys. Rev. B* **56**, 8945 (1997).
- [23] E. Luijten and H. W. J. Blöte, *Phys. Rev. Lett.* **89**, 025703 (2002).
- [24] T. Horita, H. Suwa, and S. Todo, *Phys. Rev. E* **95**, 012143 (2017).
- [25] A. Hucht, A. Moschel, and K. Usadel, *J. Magn. Mater.* **148**, 32 (1995).
- [26] D. Frenkel and B. Smit, *Understanding Molecular Simulations: From Algorithms to Applications* (Academic, New York, 2002).
- [27] P. Ewald, *Ann. Phys. (Leipzig)* **369**, 253 (1921).
- [28] R. Burioni, D. Cassi, F. Corberi, and A. Vezzani, *Phys. Rev. E* **75**, 011113 (2007).
- [29] F. Corberi, E. Lippiello, and M. Zannetti, *Phys. Rev. E* **74**, 041106 (2006).
- [30] H. Christiansen, S. Majumder, and W. Janke, *arXiv:2011.06098*.
- [31] F. Corberi, E. Lippiello, and P. Politi, *Europhys. Lett.* **119**, 26005 (2017).
- [32] R. Livi and P. Politi, *Nonequilibrium Statistical Physics: A Modern Perspective* (Cambridge University Press, Cambridge, 2017).
- [33] A. D. Rutenberg, *Phys. Rev. E* **54**, R2181(R) (1996).
- [34] C. Günther, P. Rikvold, and M. Novotny, *Physica A* **212**, 194 (1994).